Nonlocal nonlinear optical X waves and their active control in a Rydberg atomic gas

Huanhuan Xu,[1] Chao Hang [1,2,3] and Guoxiang Huang[1,2,3]

[1]*State Key Laboratory of Precision Spectroscopy, East China Normal University, Shanghai 200062, China*
[2]*NYU-ECNU Institute of Physics at NYU Shanghai, Shanghai 200062, China*
[3]*Collaborative Innovation Center of Extreme Optics, Shanxi University, Taiyuan 030006, China*

X waves are a special type of wave packet that can maintain their transverse profile of X shape during propagation, and they are of much interest for the study of fundamental physics and practical applications. Here we present a scheme to generate nonlinear X waves and realize their active control by using a cold gas of Rydberg atoms via electromagnetically induced transparency (EIT). We show that, due to the EIT effect contributed by a control laser field and the strong, nonlocal Kerr nonlinearity contributed by Rydberg-Rydberg interaction between atoms, the system supports high-dimensional, nonlocal, and nonlinear optical X waves, which have low propagation loss, ultraslow propagation velocity, and ultralow generation power. We also show that the stability domain of such X waves can be greatly enlarged by increasing the nonlocality degree of the Kerr nonlinearity, and their motion trajectory can be manipulated by using an external magnetic field. Our study opens a route for generating and controlling nonlocal ultraslow nonlinear optical X waves, which may have promising applications in optical information processing and transmission.

I. INTRODUCTION

X waves are a special type of wave packet that can keep their transverse profiles of characteristic X shape during propagation [1,2]. The formation of such wave packets can be understood as nonmonochromatic superpositions of plane waves with the same wave vector along the propagation direction. Different from solitons [3–5], X waves can propagate free from diffraction or dispersion even in the absence of nonlinearity. Moreover, in some sense X waves are more robust than solitons because the latter ones are usually unstable when propagating in high dimensions. However, to generate X waves the dispersion relation of a system must be hyperbolic; i.e., the effective mass has the opposite sign in transverse directions.

Due to their unique features described above, X waves and related topics have attracted intense attention in recent years [6]. Particularly, optical X waves have been investigated and observed in various physical systems including fluids [7,8] and optical media [9–25]. Besides, X waves have also been studied in many other systems, such as acoustic materials [26], condensed matters [27,28], polariton fluids [29–31], and so on. Except for the fundamental interest in wave localization, the research on X waves has facilitated many important applications, including high frame-rate medical and optical imaging, high-quality optical lithography tweezers and tomography, high-capacity communications from microwave to optical waves, etc. [6,32,33].

Although nonlinearity is not required for sustaining the wave shape of X waves, it may play an important role in their formation and propagation. It has been shown that nonlinear X waves can be generated spontaneously by using simple Gaussian input pulses or other input pulses through a self-induced spectral reshaping mechanism [6]. Among X waves

considered in various nonlinear systems, there is growing interest in the study of nonlinear optical X waves (NLOXWs) [9–11,14,15]. Yet, up to now all the NLOXWs have been obtained by using passive optical media, which have the propagation speed closed to c (i.e., the light speed in vacuum) and have high generation power due to nonresonant (thus small) Kerr nonlinearity; furthermore, such NLOXWs are hard to control and manipulate actively.

In this work, we propose a scheme to produce a different type of nonlinear X wave and realize its active control. The system we consider is a cold Rydberg atomic gas [34–38], where a Λ-type electromagnetically induced transparency (EIT) [39] is adopted and the EIT is dressed by a Rydberg state, which brings interatomic interaction (also called Rydberg-Rydberg interaction) into the system. We show that, due to the contribution from the EIT and the nonlocal Kerr nonlinearity induced by the Rydberg-Rydberg interaction, the system supports high-dimensional, low-loss, nonlocal NLOXWs with ultraslow propagation velocity and extremely low generation power. Similar to the nonlocal solitons considered in Refs. [40–52], we clarify the effect of the nonlocal Kerr nonlinearity acting on the formation, propagation, and stabilization of such NLOXWs.

We stress that the NLOXWs found here are different from those reported before [9–25]. First, our system is based on a cold atomic gas working under the condition of Rydberg-EIT. Due to the existence of the strong Rydberg-Rydberg interaction, the NLOXWs obtained are nonlocal nonlinear optical wave packets, which have ultraslow propagation velocity ($\sim 10^{-3}c$) and ultralow generation power (with the order of several nanowatts). Second, the nonlinear X waves in our system can be well manipulated due to the active character of the system; in particular, their stability domain may be

largely enlarged by increasing the nonlocality degree of the Kerr nonlinearity. Third, the nonlinear *X* waves obtained here may experience a significant deflection by using an external magnetic field; inversely, the external magnetic field can be measured by the motion trajectory of the nonlinear *X* waves, which can be exploited for the precision measurement of magnetic fields. All these properties of the NLOXWs are absent for the nonlinear *X* waves considered previously [9–25]. Our study opens a way for generating and actively controlling nonlocal NLOXWs, which may have promising applications in precision measurement and in optical information processing and transmission.

The remainder of the article is arranged as follows. In Sec. II, we describe the physical model under study and derive a $(3 + 1)$-dimensional $[(3 + 1)D]$ nonlinear envelope equation controlling the evolution of the wave packet of the probe laser field. In Sec. III, we investigate the formation and stability of $(3 + 1)D$ nonlocal NLOXWs. In Sec. IV, we discuss how to actively control the motion trajectory of the NLOXWs by using an external magnetic field. Finally, in Sec. V we summarize the main results obtained in this work.

II. MODEL AND NONLINEAR ENVELOPE EQUATION

A. Physical model

We start to consider a cold, lifetime-broadened four-level atomic gas with an inverted-Y type-configuration, shown in Fig. 1(a). The electric field resonantly interacting with the atomic gas reads $\mathbf{E} = \mathbf{E}_p + \mathbf{E}_c + \mathbf{E}_a$, with $\mathbf{E}_\alpha = \mathbf{e}_\alpha \mathcal{E}_\alpha \exp[i(\mathbf{k}_\alpha \cdot \mathbf{r} - \omega_\alpha t)] + \text{H.c.}$ and $\mathbf{r} = (x, y, z)$. Here $\mathbf{e}_\alpha$ are unit polarization vectors, $\mathcal{E}_\alpha$ are field amplitudes ($\alpha = p, c, a$), and H.c. represents the corresponding complex conjugate. The probe field $\mathbf{E}_p$ (with wave number $k_p = \omega_p/c$, angular frequency ω_p, and half Rabi frequency Ω_p) is weak, is pulsed, and couples the ground state $|1\rangle$ to the intermediate state $|3\rangle$; the control field $\mathbf{E}_c$ (with wave number $k_c = \omega_c/c$, angular frequency ω_c, and half Rabi frequency Ω_c) is strong, is continuous, and couples the low-lying state $|2\rangle$ and the state $|3\rangle$. In the level diagram, Δ_3 is a one-photon detuning; Δ_2 and Δ_4 are two-photon detunings; and Γ_{13}, Γ_{23}, and Γ_{34} are respectively the spontaneous-emission decay rates from $|3\rangle$ to $|1\rangle$, $|3\rangle$ to $|2\rangle$, and $|4\rangle$ to $|3\rangle$. States $|1\rangle$, $|2\rangle$, and $|3\rangle$ and the probe and control fields constitute a standard EIT configuration. The Λ-type EIT is, however, dressed by a high-lying Rydberg state $|4\rangle$ (with a large principal quantum number n), which is far off-resonantly (i.e., $\Delta_3 + \Delta_4 \gg \Omega_a$) coupled to $|3\rangle$ through an assistant laser field $\mathbf{E}_a$ (with wave number $k_a = \omega_a/c$, angular frequency ω_a, and half Rabi frequency Ω_a). The reason for using Rydberg-dressed EIT is to exploit the advantages of EIT (which can suppress the absorption of the probe field due to the spontaneous emission) and the Rydberg state (which can provide a giant nonlocal Kerr nonlinearity contributed by the Rydberg-Rydberg interaction), simultaneously.

The dynamics of the system is described by the Hamiltonian $\hat{H} = \mathcal{N}_a \int d^3 r \hat{\mathcal{H}}(\mathbf{r}, t)$, with $\hat{\mathcal{H}}(\mathbf{r}, t)$ being the Hamiltonian density and $\mathcal{N}_a$ the atom density. Under electric-dipole and rotating-wave approximations, the Hamiltonian density in
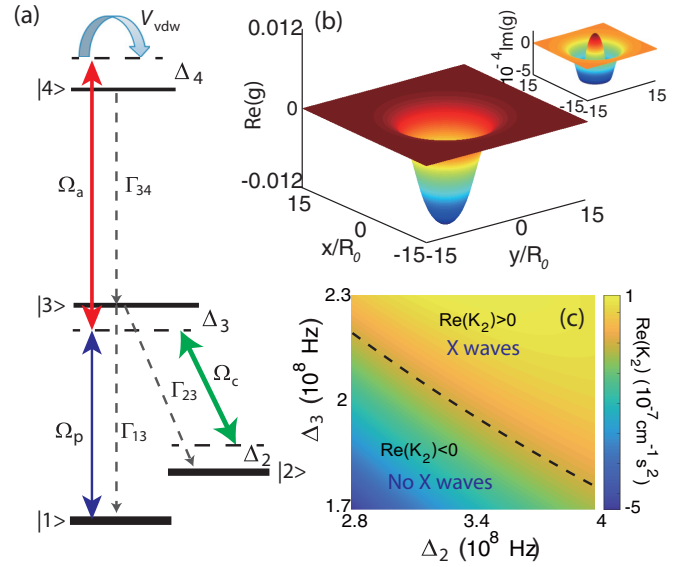
FIG. 1. (a) Level diagram and excitation scheme of the Rydberg-dressed EIT. Ω_p, Ω_c, and Ω_a are half Rabi frequencies of the probe, control, and assisted laser fields, respectively. Δ_α are detunings and $\Gamma_{\alpha\beta}$ are spontaneous-emission decay rates from $|\beta\rangle$ to $|\alpha\rangle$, respectively. The interaction between Rydberg atoms is described by the van der Waals potential $V_{\text{vdw}} \equiv \hbar V(\mathbf{r}' - \mathbf{r})$, with $V(\mathbf{r}' - \mathbf{r}) = C_6/|\mathbf{r}' - \mathbf{r}|^6$ (C_6 is called the dispersion parameter). (b) Spatial distributions of the real and imaginary parts of the dimensionless nonlocal nonlinear response g, i.e., $\text{Re}(g)$ and $\text{Im}(g)$, in the plane of x/R_0 and y/R_0. (c) The real part of group velocity dispersion K_2, i.e., $\text{Re}(K_2)$, as a function of Δ_2 and Δ_3. The dashed line is the one for $\text{Re}(K_2) = 0$. Nonlocal nonlinear optical *X* waves are allowed (not allowed) in the region for $\text{Re}(K_2) > 0$ [$\text{Re}(K_2) < 0$].

the interaction picture reads

$$
\begin{aligned}
\hat{\mathcal{H}}(\mathbf{r}, t) = &-\hbar \sum_{j=2}^{4} \Delta_\alpha \hat{S}_{\alpha\alpha}(\mathbf{r}, t) - \hbar[\Omega_p \hat{S}_{13}(\mathbf{r}, t) \\
&+ \Omega_a \hat{S}_{34}(\mathbf{r}, t) + \Omega_c \hat{S}_{23}(\mathbf{r}, t) + \text{H.c.}] \\
&+ \mathcal{N}_a \int d^3 r \int d^3 r' \, \hat{S}_{44}(\mathbf{r}', t) \hbar V(\mathbf{r}' - \mathbf{r}) \hat{S}_{44}(\mathbf{r}, t),
\end{aligned}
$$

(1)

where $d^3 r = dx\, dy\, dz$, and $\hat{S}_{\alpha\beta}(\mathbf{r}, t) = |\beta\rangle\langle\alpha| \exp\{i[(\mathbf{k}_\beta - \mathbf{k}_\alpha) \cdot \mathbf{r} - (\omega_\beta - \omega_\alpha + \Delta_\beta - \Delta_\alpha)t]\}$ is the transition operator related to the states $|\alpha\rangle$ and $|\beta\rangle$, satisfying the commutation relation

$$
\begin{aligned}
&[\hat{S}_{\alpha\beta}(\mathbf{r}, t), \hat{S}_{\mu\nu}(\mathbf{r}', t)] \\
&= \frac{1}{\mathcal{N}_a} \delta(\mathbf{r} - \mathbf{r}')[\delta_{\alpha\nu}\hat{S}_{\mu\beta}(\mathbf{r}', t) - \delta_{\mu\beta}\hat{S}_{\alpha\nu}(\mathbf{r}', t)].
\end{aligned}
$$

(2)

Here $\hbar\omega_\alpha$ is the eigenenergy of the level $|\alpha\rangle$; $\Delta_3 = (\omega_3 - \omega_1) - \omega_p$ is a one-photon detuning, $\Delta_2 = \omega_p - \omega_c - (\omega_2 - \omega_1)$ and $\Delta_4 = \omega_p + \omega_a - (\omega_4 - \omega_1)$ are two-photon detunings; and $\Omega_p = (\mathbf{e}_p \cdot \mathbf{p}_{31})\mathcal{E}_p/\hbar$, $\Omega_c = (\mathbf{e}_c \cdot \mathbf{p}_{32})\mathcal{E}_c/\hbar$, and $\Omega_a = (\mathbf{e}_a \cdot \mathbf{p}_{43})\mathcal{E}_a/\hbar$ are respectively half Rabi frequencies of the probe, control, and assistant fields, with $\mathbf{p}_{\alpha\beta}$ being the electric dipole matrix elements associated with the transition $|\alpha\rangle \leftrightarrow |\beta\rangle$. The last term in the Hamiltonian density is the

contribution coming from the Rydberg-Rydberg interaction, where the two-body potential is of the van der Waals form $V_{\text{vdw}} \equiv \hbar V(\mathbf{r}' - \mathbf{r}) = \hbar C_6/|\mathbf{r}' - \mathbf{r}|^6$ (C_6 is dispersion parameter, which may be positive or negative).

From the Hamiltonian given above, we obtain the optical Bloch equation

$$\frac{\partial \rho}{\partial t} = -\frac{i}{\hbar}[\hat{H}, \rho] - \Gamma[\rho], \quad (3)$$

where ρ is the density matrix, with matrix elements $\rho_{\alpha\beta} \equiv \langle \hat{S}_{\alpha\beta} \rangle$ [53], and Γ is a relaxation matrix, contributed by the spontaneous emission and dephasing. The explicit form of Eq. (3) is given in the Appendix.

The evolution of the probe field is controlled by the Maxwell equation, which under the slowly varying amplitude approximation reads

$$i\left(\frac{\partial}{\partial z} + \frac{1}{c}\frac{\partial}{\partial t}\right)\Omega_p + \frac{1}{2k_p}\left(\frac{\partial^2}{\partial x^2} + \frac{\partial^2}{\partial y^2}\right)\Omega_p + \kappa_{13}\rho_{31} = 0, \quad (4)$$

where $\kappa_{13} = \mathcal{N}_\alpha (\mathbf{e}_p \cdot \mathbf{p}_{13})^2 \omega_p/(2\varepsilon_0 \hbar c)$ is a constant describing the coupling between the probe field and the atomic gas. For convenience and without loss of generality, the propagation direction of the probe field is assumed to be along the z direction, i.e., $\mathbf{k}_p = (0, 0, k_p)$; furthermore, in order to suppress the Doppler effect, the wave vectors of the control and assisted fields are taken to be along, respectively, the positive and negative z directions, [i.e., $\mathbf{k}_c = (0, 0, k_c)$ and $\mathbf{k}_a = (0, 0, -k_a)$].

B. Nonlinear envelope equation

We now derive the nonlinear equation that describes the nonlinear evolution of the probe-field envelope beyond the mean-field approximation. We assume that atoms are initially populated only in the ground state $|1\rangle$. Since the probe field is weak, the population in atomic levels changes not much when the probe field is applied to the system, and hence a method of multiple scales [3,52,54,55] can be employed to solve the Maxwell-Bloch (MB) equations (3) and (4). To be concrete, we employ the asymptotic expansions $\Omega_p = \epsilon\Omega_p^{(1)} + \epsilon^2\Omega_p^{(2)} + \cdots$ and $\rho_{\alpha\beta} = \rho_{\alpha\beta}^{(0)} + \epsilon\rho_{\alpha\beta}^{(1)} + \cdots$, where ϵ is a small parameter characterizing the typical amplitude of the probe field and multiple scale variables $z_j = \epsilon^j z$ ($j = 0, 1, 2$), $t_j = \epsilon^j t$ ($j = 0, 1$), $x_1 = \epsilon x$, and $y_1 = \epsilon y$. Substituting expansions in Eqs. (3) and (4) and comparing powers of ϵ, we obtain a set of equations at different orders, which can be solved order by order.

The linear evolution of the system is described by the solution at the first-order approximation. The probe field at this order reads $\Omega_p^{(1)} = F \exp\{i[K(\omega)z_0 - \omega t_0]\}$, here F is an envelope function of the slow variables x_1, y_1, z_1, t_1, and z_2. The linear dispersion relation reads

$$K(\omega) = \omega/c - \kappa_{13}(\omega + d_{21})(\omega + d_{41})/D(\omega), \quad (5)$$

with $D(\omega) = (\omega + d_{21})(\omega + d_{31})(\omega + d_{41}) - |\Omega_a|^2(\omega + d_{21}) - |\Omega_c|^2(\omega + d_{41})$.

With the first-order solution in hand, one can go to the second- and third-order approximations. Then a (3 + 1)D

envelope equation for the envelope F including diffraction, dispersion, and nonlocal Kerr nonlinearity can be obtained, which after returning to the original variables has the form

$$i\frac{\partial U}{\partial z} = -\frac{1}{2k_p}\nabla_\perp^2 U + \frac{K_2}{2}\frac{\partial^2 U}{\partial T^2}$$
$$+ \int d^3 r' H(\mathbf{r} - \mathbf{r}')|U(\mathbf{r}', T)|^2 U(\mathbf{r}, T) - i\frac{\alpha_0}{2}U, \quad (6)$$

with $\nabla_\perp^2 = \partial^2/\partial x^2 + \partial^2/\partial y^2$, $U = \epsilon F \exp(-i\alpha_0 z)$, $\alpha_0 = \text{Im}(K)$, and $T = t - z/V_g$. Here, $V_g = (\partial K/\partial \omega)^{-1}$ is the group velocity, $K_2 = \partial^2 K/\partial \omega^2$ is the group velocity dispersion, and $H(\mathbf{r} - \mathbf{r}') = \kappa_{13}\mathcal{N}_a d_{21}\Omega_a^* a_{44,41}^{(3)}(\mathbf{r}', \mathbf{r})/D$ is the nonlinear response function contributed by the Rydberg-Rydberg interaction. The detailed derivation of the nonlocal nonlinear Schrödinger (NLS) equation (6) and the explicit expression of $a_{44,41}^{(3)}$ are presented in Appendix. Notice that (i) for avoiding the excitation of other atomic states, the spectral width of the probe field is assumed to be narrow enough (the spectral width of the probe field is $\sim 10^7$ Hz, which is smaller by 8 orders of magnitude when compared with the central frequency of the probe field, $\omega_p \sim 10^{15}$ Hz), so the expressions of V_g, K_2, H, and α_0 have been simplified by taking $\omega = 0$, and (ii) due to the EIT effect, the imaginary parts of V_g and K_2 are much smaller than their corresponding real parts, i.e., $V_g = \text{Re}(V_g) + i\text{Im}(V_g) \approx \text{Re}(V_g)$ and $K_2 = \text{Re}(K_2) + i\text{Im}(K_2) \approx \text{Re}(K_2)$, and they can be neglected.

C. Explicit form of the nonlinear response function

For simplification of the following discussions, we assume that the typical length of the probe-field envelope is much larger than the range of Rydberg-Rydberg interaction, so that a local approximation along the z direction can be made. In this situation, the last term on the left-hand side of Eq. (6) can be reduced to the form $\iint dx'dy' G(\mathbf{r}_\perp - \mathbf{r}_\perp')|U(\mathbf{r}_\perp', z)|^2 U(\mathbf{r}_\perp, z)$, where $\mathbf{r}_\perp \equiv (x, y)$, and $G(\mathbf{r}_\perp - \mathbf{r}_\perp') \equiv \int dz H(\mathbf{r}_\perp - \mathbf{r}_\perp', z)$ is the reduced response function.

In the following calculations, a cold gas of ^{88}Sr atoms is chosen. The atomic levels are assigned to be $|1\rangle = |5S_{1/2}, F = 1\rangle$, $|2\rangle = |5S_{1/2}, F = 2\rangle$, $|3\rangle = |5P_{3/2}, F = 3\rangle$, and $|4\rangle = |nS_{1/2}\rangle$, with n being the principle quantum number. The parameters of the system are given by $\Gamma_2 = 2\pi \times 10$ kHz, $\Gamma_3 = 2\pi \times 16$ MHz, $\Gamma_4 = 2\pi \times 16.7$ kHz, $\Delta_2 = 10$ MHz, $\Delta_3 = 350$ MHz, $\Delta_4 = 15$ MHz. $\Omega_c = 100$ MHz, $\Omega_a = 60$ MHz, $\mathcal{N}_a = 1.0 \times 10^{10}$ cm^{-3} (corresponding to $\kappa_{13} = 4.35 \times 10^7$ cm^{-1} Hz), and $C_6 = -2\pi \times 81.6$ GHz μm^6 (for $n = 60$) [56]. With these parameters, we obtain the explicit expression of the reduced nonlinear response function:

$$G(\mathbf{r}_\perp - \mathbf{r}_\perp') \approx -(24.25 + i4.00)$$
$$\times \int dz \left\{ 1 + i0.22 + \frac{[(\mathbf{r}_\perp - \mathbf{r}_\perp')^2 + z^2]^3}{(1.01R_b)^3} \right\}^{-1}. \quad (7)$$

Here $R_b \equiv (|C_6|/|\delta_{\text{EIT}}|)^{1/6}$ is the radius of the Rydberg blockade, with $\delta_{\text{EIT}} \equiv |\Omega_c|^2/|\Delta_3 + i\gamma_{31}|$ being the linewidth of the

EIT transmission spectrum (or the width of the EIT transparency window). Based on the above parameters, under our consideration $R_b \approx 5.1$ μm; in addition, since G is negative, the nonlocal Kerr nonlinearity of the system is a self-focusing one.

For convenience, we write Eq. (6) in the dimensionless form

$$i\frac{\partial u}{\partial s} = -\beta_0 \tilde{\nabla}_\perp^2 u + \rho_0 \frac{\partial^2 u}{\partial \tau^2} + \iint d^2 \zeta' g(\vec{\zeta} - \vec{\zeta}')|u(\vec{\zeta}', \tau)|^2$$
$$\times u(\vec{\zeta}, \tau) - i\gamma_0 u, \qquad (8)$$

with $u = U/U_0$, $s = z/(2L_{\text{disp}})$, $\vec{\zeta} = (\xi, \eta) = (x, y)/R_0$, $\tilde{\nabla}_\perp^2 = \partial^2/\partial\xi^2 + \partial^2/\partial\eta^2$, $\tau = t/\tau_0$, $\beta_0 = L_{\text{disp}}/L_{\text{diff}}$, $\rho_0 = \text{sgn}[\text{Re}(K_2)]$, $\gamma_0 = L_{\text{disp}}/L_{\text{abs}}$, and $d^2\zeta' = d\xi'd\eta'$. Here R_0, U_0, and τ_0 are respectively the typical transverse size, Rabi frequency, and pulse duration of the probe field; $L_{\text{disp}} \equiv \tau_0^2/|\text{Re}(K_2)|$, $L_{\text{diff}} \equiv \omega_p R_0^2/c$, and $\gamma_0 = L_{\text{disp}}/L_{\text{abs}}$ (with $L_{\text{abs}} \equiv 1/\alpha_0$) are respectively the typical dispersion, diffraction, and absorption lengths; and $\text{sgn}[\text{Re}(K_2)]$ is a sign function of $\text{Re}(K_2)$, i.e., $\text{sgn}[\text{Re}(K_2)] = 1$ $(= -1)$ when $\text{Re}(K_2) > 0$ $[\text{Re}(K_2) < 0]$. The dimensionless response function in Eq. (8) is defined by $g(\vec{\zeta}) = 4\tau_0^4 R_0^2 G(\vec{\zeta})|U_0|^2/[\text{Re}(K_2)]^2$, reading as

$$g(\vec{\zeta}) \approx -(1.12 + i0.19) \times 10^{-3} g_0 \int ds \left\{ 1 + i0.22 + \frac{[(\vec{\zeta} - \vec{\zeta}')^2 + 4\tau_0^4 s^2/[\text{Re}(K_2)^2 R_0^2]]^3}{(1.01 R_b/R_0)^6} \right\}^{-1}, \qquad (9)$$

where $g_0 = \iint d^2\zeta' g(\vec{\zeta} - \vec{\zeta}')$ is a nonlinear parameter characterizing the magnitude of the nonlocal Kerr nonlinearity. Figure 1(b) shows the shape of g as a function of ξ and η. One sees that the imaginary part $\text{Im}(g)$ is much smaller than the real part $\text{Re}(g)$.

The nonlocal property of the Kerr nonlinearity can be characterized by its nonlocality degree, defined by

$$\sigma \equiv R_b/R_0. \qquad (10)$$

When the transverse size of the probe pulse is much larger than the radius of the Rydberg blockade, i.e., $R_0 \gg R_b$, one has $\sigma \approx 0$, in which case the nonlocal Kerr nonlinearity becomes a local one and the nonlocal NLS equation (8) is reduced to a NLS equation with a local Kerr nonlinearity. However, if $R_0 \ll R_b$, the nonlocal effect of the Kerr nonlinearity plays a significant role in the propagation and stability of high-dimensional probe pulses.

III. NONLOCAL NONLINEAR X WAVES AND THEIR STABILITY

A. Formation of nonlinear X waves

We now turn to consider the formation and propagation of NLOXWs in the system. Since the system is actively controllable, we can adjust the sign and the magnitude of K_2 (i.e., the group velocity dispersion) through tuning the one- and two-photon detunings Δ_2 and Δ_3. In order to realize NLOXWs, one must have $\text{Re}(K_2) > 0$, and hence $\rho_0 = 1$. Shown in Fig. 1(c) is the result of $\text{Re}(K_2)$ as a function of Δ_2 and Δ_3. The dashed line in the figure is the one for $\text{Re}(K_2) = 0$. NLOXWs are allowed (not allowed) in the region for $\text{Re}(K_2) > 0$ $[\text{Re}(K_2) < 0]$.

Based on the system parameters given in the last subsection along with the pulse duration $\tau_0 \approx 0.3 \times 10^{-7}$ s, we have $L_{\text{disp}} \approx L_{\text{diff}} = 1.6$ cm and $L_{\text{abs}} = 197$ cm, and hence $\beta_0 = 1$ and $\gamma_0 \approx 0$. As a result, Eq. (8) is reduced to

$$i\frac{\partial u}{\partial s} = -\tilde{\nabla}_\perp^2 u + \frac{\partial^2 u}{\partial \tau^2} + \iint d^2\zeta' g(\vec{\zeta} - \vec{\zeta}')|u(\vec{\zeta}', s)|^2 u(\vec{\zeta}, s).$$
$$(11)$$

Equation (11) is now a hyperbolic one with nonlocal Kerr nonlinearity; in the linear regime (i.e., $g_0 = 0$), which is valid for the very low probe-field intensity, it admits the s-independent X wave solution

$$u = \frac{1}{\sqrt{(\xi^2 + \eta^2) + (\delta_0 - i\tau)^2}}, \qquad (12)$$

where δ_0 is a free parameter, characterizing the localization degree of the solution; i.e., the smaller δ_0 is, the stronger the localization of the X wave is.

The linear X wave solution [Eq. (12)] describes an X-shaped wave packet localized in both time and transverse directions. Although such a wave can propagate stably, it cannot be generated spontaneously and its production needs a sophisticated input-beam shaping technique. To avoid such a requirement, one can introduce nonlinearity into the system, so that a nonlinear X wave is spontaneously generated via a self-induced spectral reshaping mechanism, which can be realized by using an input of simple Gaussian or other type of wave packet [6].

Based on such an idea, we carried out a numerical simulation for the formation and propagation of optical X waves in the Rydberg atomic gas in both linear and nonlinear regimes. Shown in Figs. 2(a) and 2(b) are the results of linear (i.e., $g_0 = 0$) probe pulses in the $\eta = 0$ plane as functions of $\xi = x/R_0$ and $\tau = t/\tau_0$ when propagating to $z = 2L_{\text{disp}} = 3.2$ cm, with the initial conditions respectively given by Eq. (12) and $u(s = 0) = e^{-(\xi^2 + \eta^2 + \tau^2)/4}$. We see that, compared with the case shown in Fig. 2(a) where the X wave propagates quite stably, the probe pulse with the input of a Gaussian wave packet [Fig. 2(b)] spreads out rapidly and it cannot be transformed spontaneously into an X-shaped wave during the propagation. Nevertheless, when a local Kerr nonlinearity of the system is taken into account, the probe pulse with the input of a Gaussian wave packet may transform into an X wave, i.e., NLOXW, which is illustrated in Fig. 2(c) where the magnitude of the Kerr nonlinearity and the nonlocality degree are taken to be $g_0 = 2$ and $\sigma = 0$, respectively. However, the NLOXW obtained is unstable and it generates vortices during propagation. Figure 2(d) shows the phase of the wave function for
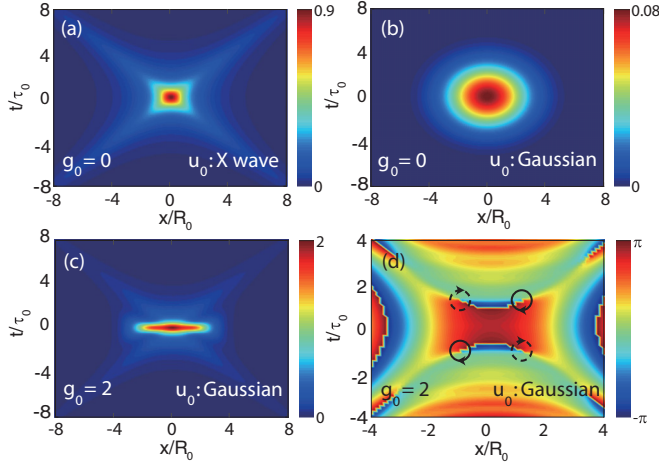
FIG. 2. Formation and propagation of local X waves. (a) Linear X wave as a function of x/R_0 and t/τ_0 when propagating to $z = 2L_{disp} = 3.2$ cm, with the initial condition given by Eq. (12). (b) The same as panel (a) but for the input of a Gaussian wave packet, with the wave function $u(s = 0) = e^{-(\xi^2+\eta^2+\tau^2)/4}$. (c) Local nonlinear X wave when propagating to $z = 2L_{disp} = 3.2$ cm, by taking a Gaussian wave packet as an input. The magnitude of the Kerr nonlinearity and the nonlocality degree are $g_0 = 2$ and $\sigma = 0$, respectively. (d) The phase of the wave function for the local nonlinear X wave. The generation of quantized vortex-antivortex pairs is indicated by the solid and dashed circles.

the local nonlinear X wave generated from a Gaussian wave packet, where quantized vortex-antivortex pairs are indicated by the solid and dashed circles.

B. Stabilization of the nonlinear X waves

The numerical result given in the last subsection shows that the NLOXWs obtained by a local Kerr nonlinearity are unstable during propagation. It is necessary to know under what conditions these waves are stable and under what conditions they are not. To acquire a "phase diagram" on the stability of NLOXWs, here we carry out a general liner stability analysis of the nonlocal NLS equation (11). To this aim, we assume $u = [u_0(\vec{\zeta}, \tau) + \tilde{f}(\vec{\zeta}, \tau) \exp(i\lambda s) + \tilde{g}^*(\vec{\zeta}, \tau) \exp(-i\lambda^* s)] \exp(iqs)$. Here $u_0(\vec{\zeta}, \tau)$ is the wave function of a nonlinear X wave, $\tilde{f}(\vec{\zeta}, \tau)$ and $\tilde{g}(\vec{\zeta}, \tau)$ denote the amplitudes of perturbations acting on the X wave, and λ is the growth rate of the perturbations. Substituting this expression in Eq. (11), we obtain the following linear eigenvalue problem:

$$\lambda \tilde{f} = \left(\tilde{\nabla}_\perp^2 - \frac{\partial^2}{\partial \tau^2} - q \right) \tilde{f} - n\tilde{f} - u_0(\vec{\zeta}, \tau)\Delta n, \quad (13a)$$

$$\lambda \tilde{g} = \left(-\tilde{\nabla}_\perp^2 + \frac{\partial^2}{\partial \tau^2} + q \right) \tilde{g} + n\tilde{g} + u_0^*(\vec{\zeta}, \tau)\Delta n, \quad (13b)$$

where $n = \iint d^2\zeta' g(\vec{\zeta} - \vec{\zeta}')|u_0(\vec{\zeta}, \tau)|^2$ and $\Delta n = \iint d^2\zeta' g(\vec{\zeta} - \vec{\zeta}')[u_0(\vec{\zeta}', \tau)\tilde{g}(\vec{\zeta}') + u_0^*(\vec{\zeta}', \tau)\tilde{f}(\vec{\zeta}')]$. Equation (13) can be solved numerically by using a plane-wave expansion method [57]. NLOXWs are stable if Im(λ) = 0 for all the eigenvalues

of λ, and they are unstable if there is at least one eigenvalue of λ at which its imaginary part is nonzero, i.e., Im(λ) ≠ 0.

Shown Fig. 3(a) is the "phase diagram" of the stability of NLOXWs in the plane of the magnitude g_0 and the nonlocality degree σ of the Kerr nonlinearity, in which the left-upper (right-lower) region is the one where NLOXWs are stable (unstable). The solid black line in the figure is the boundary between the stability and the instability regions. The inset zooms in the stability and instability regions for the interval $0 < g_0 < 2$. From the figure we obtain the following conclusions: (i) linear X waves (corresponding to $g_0 = 0$) are stable, (ii) NLOXWs are unstable for the Kerr nonlinearity with zero or small nonlocality degree σ, and (iii) NLOXWs can be stabilized by increasing the nonlocality degree σ of the Kerr nonlinearity. Particularly, the stability domain can be greatly enlarged as σ is increased. Figure 3(b) shows the intensity distribution of a stable NLOXW by taking $(g_0, \sigma) = (6, 1.3)$ [labeled by "A" in Fig. 3(a)] when it propagates to the distance $z = 2L_{disp} = 3.2$ cm. For comparison, the intensity distribution of an unstable NLOXW by taking $(g_0, \sigma) = (6, 0.2)$ [labeled by "B" in Fig. 3(a)] is illustrated in the right-lower panel of the figure. The stable NLOXW has no obvious distortion during propagation, while the unstable NLOXW deforms significantly and its intensity maximum is increased by three times compared with that of its input.

The propagation speed of the stable NLOXW is mainly determined by the group velocity of the probe-pulse envelope. Based on the system parameters given above, we obtain

$$V_g \approx 4.4 \times 10^{-3} c, \quad (14)$$

which is very slow compared with c (the light speed in vacuum), resulting from the EIT effect in the system. The threshold of the optical power P_{th} for generating the NLOXW

FIG. 3. (a) "Phase diagram" of the stability and the instability of NLOXWs in the plane of the nonlinear parameter g_0 and the nonlocality degree σ of the Kerr nonlinearity. The solid black line is the boundary between the stability and the instability regions. The inset zooms in the stability and instability regions for the interval $0 < g_0 < 2$. (b) Light intensity distribution of a stable NLOXW as a function of x/R_0 and t/τ_0 when the NLOXW propagates to $z = 2L_{disp} = 3.2$ cm, by taking $(g_0, \sigma) = (6, 1.3)$ [labeled by the point "A" in the stable region of panel (a)]. (c) The same as panel (b) but for an unstable NLOXW, by taking $(g_0, \sigma) = (6, 0.2)$ [labeled by the point "B" in the unstable region of panel (a)].

can be estimated by estimating the Poynting's vector [3,52]. Taking into account that the typical half Rabi frequency U_0 of the probe pulse is about 1 order of magnitude smaller than Ω_c, i.e., $U_0 \sim 10^6$ Hz, together with the cross-section area of the probe pulse, ~ 0.02 mm^2, we obtain

$$P_{\text{th}} \approx 1.8 \text{ nW}. \tag{15}$$

We see that a very low input power is needed to generate NLOXWs in the present system. The reason is that the system has largely enhanced Kerr nonlinearity due to the Rydberg-Rydberg interaction. Thereby, the NLOXWs proposed here are completely different from those nonlinear X waves obtained by using other passive optical media, which have the propagation speed very close to c and require a very high generation power in order to bring enough nonlinear effect to trigger the self-induced spectral reshaping for the formation of NLOXWs [6,9,11].

IV. ACTIVE MANIPULATION OF THE NONLINEAR X WAVES

A. External potential induced by a gradient magnetic field

Last, we study the active manipulation of the nonlocal NLOXWs in the system. As an example, we assume that a gradient magnetic field is applied to the atomic gas along the z direction, with the form

$$\mathbf{B}(x, y) = \hat{\mathbf{z}} B(\mathbf{r}_\perp) = \hat{\mathbf{z}}(B_1 x + B_2 y), \tag{16}$$

where $\hat{\mathbf{z}}$ is the unit vector in the z direction, and B_1 and B_2 characterize the gradients of the magnetic field along the x and y directions, respectively. Due to the presence of the magnetic field, each atomic level is split into a series of Zeeman sublevels with the energy $\Delta E_{\text{Zeeman}} = \mu_B g_F^\alpha m_F^\alpha B$, where μ_B, g_F^α, and m_F^α are the Bohr magneton, the gyromagnetic factor, and the magnetic quantum number of level $|\alpha\rangle$, respectively. As a result, the one- and two-photon detunings Δ_2 and Δ_3 are changed into $\Delta_2(\mathbf{r}_\perp) = (\omega_p - \omega_c - \omega_{21}) + \mu_{21}B(\mathbf{r}_\perp)$ and $\Delta_3(\mathbf{r}_\perp) = (\omega_p - \omega_{31}) + \mu_{31}B(\mathbf{r}_\perp)$, with $\mu_{\alpha\beta} = \mu_B(g_F^\alpha m_F^\alpha - g_F^\beta m_F^\beta)/\hbar$.

The nonlinear envelope equation in the presence of the gradient magnetic field can also be derived by means of the multiple-scale perturbation method [58], which has the same form as Eq. (6), except that an additional term, $-P(\mathbf{r}_\perp)U$, appears on the right-hand side of the equation. Here

$$P(\mathbf{r}_\perp) = \kappa_{13} \frac{|\Omega_c|^2 \mu_{21} + d_{21}^{(0)\,2} \mu_{31}}{\left(|\Omega_c|^2 - d_{21}^{(0)} d_{31}^{(0)}\right)^2} (B_1 x + B_2 y) \tag{17}$$

plays the role of an external potential, contributed by the gradient magnetic field. Then the dimensionless form of the nonlinear envelope equation in the presence of the magnetic field is given as

$$i\frac{\partial u}{\partial s} = -\frac{1}{2}\left(\tilde{\nabla}_\perp^2 - \frac{\partial^2}{\partial \tau^2}\right)u - Q(\vec{\zeta})u$$
$$+ \iint d^2\zeta' g(\vec{\zeta} - \vec{\zeta}')|u(\vec{\zeta}', s)|^2 u - i\gamma_0 u, \tag{18}$$

where $Q(\vec{\zeta}) = Q_1\xi + Q_2\eta$ is the dimensionless external potential, with

$$Q_1 = \kappa_{13} \frac{|\Omega_c|^2 \mu_{21} + d_{21}^2 \mu_{31}}{(|\Omega_c|^2 - d_{21}d_{31})^2} L_{\text{disp}} R_0 B_1,$$

$$Q_2 = \kappa_{13} \frac{|\Omega_c|^2 \mu_{21} + d_{21}^2 \mu_{31}}{(|\Omega_c|^2 - d_{21}d_{31})^2} L_{\text{disp}} R_0 B_2. \tag{19}$$

B. Transverse deflection of the nonlocal nonlinear X waves

We now show that the gradient magnetic field can be used to actively control the motion of the nonlocal NLOXWs. To demonstrate this, we first consider Eq. (18) in the absence of the optical Kerr nonlinearity (i.e., $g_0 = 0$) and in the low-loss limit (i.e., $\gamma_0 \approx 0$, which is true due to the EIT effect). Using the transformation $u = u' \exp[i(Q_1\xi' + Q_2\eta' + Q_1^2 s^2/3 + Q_2^2 s^2/3)s]$, with $\xi' = \xi - Q_1 s^2/2$ and $\eta' = \eta - Q_2 s^2/2$, Eq. (18) is converted into the form $i\partial u'/\partial s = -(1/2)(\partial^2/\partial\xi'^2 + \partial^2/\partial\eta'^2 - \partial^2/\partial\tau^2)u'$, which admits the exact X wave solution

$$u = \frac{e^{-i[Q_1(\xi - Q_1 s^2/2) + Q_2(\eta - Q_2 s^2/2) + Q_1^2 s^2/3 + Q_2^2 s^2/3]s}}{\sqrt{(\xi - Q_1 s^2/2)^2 + (\eta - Q_2 s^2/2)^2 + (\varrho_0 - i\tau)^2}} \tag{20}$$

when returning to the ξ-η variables, where ϱ_0 is a constant. Obviously, the position of the center of the X wave in the ξ-η plane is given by $(\xi, \eta) = (Q_1 s^2/2, Q_2 s^2/2)$. Returning to the original x-y-z variables, the position of the center reads

$$(x, y) = \kappa_{13} \frac{|\Omega_c|^2 \mu_{21} + d_{21}^{(0)\,2} \mu_{31}}{8\left(|\Omega_c|^2 - d_{21}^{(0)} d_{31}^{(0)}\right)^2} \frac{R_0^2}{L_{\text{disp}}} z^2 (B_1, B_2). \tag{21}$$

We see that, due to the presence of the magnetic field, the motion of the X wave is changed and its trajectory in the x-y plane has a deflection with a quadratic dependence on the propagation coordinate z; moreover, the trajectory can be controlled by tuning the gradient of the magnetic field, i.e., by manipulating the parameters B_1 and B_2.

In the presence of the nonlocal Kerr nonlinearity (i.e., nonlinearity parameter $g_0 \neq 0$), an exact X wave solution is not possible. However, we can solve Eq. (18) numerically to obtain the trajectory deflection of NLOXW. Shown in the upper part of Fig. 4(a) are three-dimensional motion trajectories of a NLOXW for the nonlinear parameter $g_0 = 1$ as functions of x/R_0, y/R_0, and z/L_{disp} in the presence of the gradient magnetic field; the solid red line (trajectory A), the dashed blue line (trajectory B), and the dotted green line (trajectory C) are for $(B_1, B_2) = (50, 0)$ G cm^{-1}, $(0, 50)$ G cm^{-1}, and $(50, 50)$ G cm^{-1}, respectively. The lower part of the figure shows the light-intensity distributions of the NLOXW in the x-y plane; the left, middle, and right panels are for trajectories A, B, and C in the upper part when the NLOXW propagates to $z \equiv 2L_{\text{disp}} = 3.2$ cm. From the figure, one can see that the NLOXW experiences indeed a trajectory deflection due to the role played by the magnetic field; furthermore, the trajectory can be changed significantly by using different gradients (i.e., different B_1 and B_2) of the magnetic field.

Shown in Fig. 4(b) is the deflection of the central position of the NLOXW in the x direction as a function of z/L_{disp} (left panel) and B_1 (right panel). The dashed red line in the figure is obtained by the analytical solution (21); the blue circles and
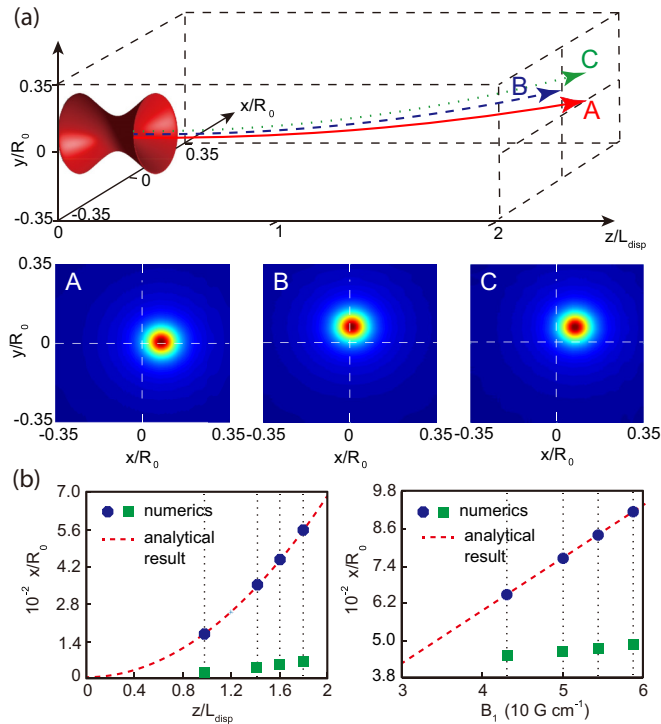
FIG. 4. Trajectory deflection of the nonlocal nonlinear *X* waves. (a) Upper part: Three-dimensional motion trajectories of a NLOXW for the nonlinear parameter $g_0 = 1$ as functions of x/R_0, y/R_0, and z/L_{disp} in the presence of the gradient magnetic field. The solid red line (trajectory A), dashed blue line (trajectory B), and dotted green line (trajectory C) are for $(B_1, B_2) = (50, 0)$ G cm^{-1}, $(0, 50)$ G cm^{-1}, and $(50, 50)$ G cm^{-1}, respectively. Lower part: Light-intensity distributions of the NLOXW in the *x*-*y* plane. The left, middle, and right panels are for trajectories A, B, and C in the upper panel when the NLOXW propagates to $z \equiv 2L_{disp} = 3.2$ cm. (b) Deflection of the central position of the NLOXW in the *x* direction as a function of z/L_{disp} (left panel) and B_1 (right panel), where the dashed red line is obtained by the analytical solution (21). Blue circles and green rectangles are respectively for the nonlocality degree of the Kerr nonlinearity $\sigma = 0$ and $\sigma = 10$, obtained numerically by solving Eq. (18) numerically.

green rectangles are respectively for the nonlocality degree of the Kerr nonlinearity $\sigma = 0$ and $\sigma = 10$, obtained numerically by solving Eq. (18) numerically. We see that the position deflection of the NLOXW in the presence of local Kerr nonlinearity (i.e., $\sigma = 0$), shown by the blue circles, is the same as that of the linear *X* wave solution (21) (shown by the red dashed lines). In particular, the position of the NLOXW may have a displacement of 3.2 μm when $B_1 = 50$ G cm^{-1} for the propagation distance $z \approx 3.2$ cm, corresponding to the deflection angle around $\approx 10^{-4}$ rad. Note that this deflection angle is 1 order of magnitude larger than that obtained in Ref. [59]. The physical reason for such large deflection is contributed by the EIT effect in the system [59–61]. As a potential application, the significant deflection of the NLOXW can be used in the precision measurement of external magnetic fields.

We have also carried out a numerical simulation on the position deflection of the NLOXW for a large nonlocality degree of the Kerr nonlinearity by taking $\sigma = 10$, with the result plotted by the green rectangles in Fig. 4(b). One sees that in this case the deflection of the NLOXW is greatly reduced. The physical reason behind this can be understood as follows. For a large nonlocal Kerr nonlinearity, all the photons in the probe pulse see almost the same Rydberg-Rydberg interaction, and hence the nonlocal nonlinear term in Eq. (18) may be reduced into an effective parabolic potential of the form $V_{\mathrm{eff}}(\vec{\zeta}) = G_0 P_0 |\vec{\zeta}|^2 = G_0 P_0 (\xi^2 + \eta^2)$ (G_0 and P_0 are constants) [52], which can trap the NLOXW. As a result, the transverse deflection of the NLOXW is largely suppressed.

V. SUMMARY

In this work, we have presented a scheme for realizing NLOXWs in a cold gas of Rydberg atoms. By means of the EIT and the Rydberg-Rydberg interaction, we have shown that high-dimensional, low-loss, nonlocal NLOXWs can be generated spontaneously by using simple inputs of Gaussian pulses when the dispersion in the system takes an opposite sign compared with that of the diffraction in the transverse dimensions; moreover, such NLOXWs may propagate with ultraslow velocity and can be generated at extremely low input power due to the EIT effect and the enhanced optical Kerr nonlinearity in the system. Furthermore, we have identified the stability and instability regions of NLOXWs and found that the stability region can be enlarged by increasing the nonlocality degree of the Kerr nonlinearity. In addition, we have demonstrated that the motion trajectories of NLOXWs can be actively controlled and manipulated by using an external gradient magnetic field. Our research opens a route for generating and actively controlling NLOXWs and may have have promising applications in precision measurement and optical information processing and transmission.

APPENDIX: EXPLICIT EXPRESSION OF THE BLOCH EQUATION AND DERIVATION OF NONLINEAR ENVELOPE EQUATION

1. Explicit expression of the Bloch equation

From the Hamiltonian given in the main text, we can obtain the explicit expression of optical Bloch equation (3) for the

one-body density matrix elements $\rho_{\alpha\beta} \equiv \langle \hat{S}_{\alpha\beta} \rangle$ [53]:

$$i\frac{\partial}{\partial t}\rho_{11} - i\Gamma_{12}\rho_{22} - i\Gamma_{13}\rho_{33} - \Omega_p\rho_{13} + \Omega_p^*\rho_{31} = 0, \tag{A1a}$$

$$i\frac{\partial}{\partial t}\rho_{22} + i\Gamma_{12}\rho_{22} - i\Gamma_{23}\rho_{33} - \Omega_c\rho_{23} + \Omega_c^*\rho_{32} = 0, \tag{A1b}$$

$$i\frac{\partial}{\partial t}\rho_{33} + i\Gamma_3\rho_{33} - i\Gamma_{34}\rho_{44} + \Omega_p\rho_{13} - \Omega_p^*\rho_{31} + \Omega_c\rho_{23} - \Omega_c^*\rho_{32} - \Omega_a\rho_{34} + \Omega_a^*\rho_{43} = 0, \tag{A1c}$$

$$i\frac{\partial}{\partial t}\rho_{44} + i\Gamma_{34}\rho_{44} + \Omega_a\rho_{34} - \Omega_a^*\rho_{43} = 0, \tag{A1d}$$

$$\left(i\frac{\partial}{\partial t} + d_{21}\right)\rho_{21} + \Omega_c^*\rho_{31} - \Omega_p\rho_{23} = 0, \tag{A1e}$$

$$\left(i\frac{\partial}{\partial t} + d_{31}\right)\rho_{31} + \Omega_p(\rho_{11} - \rho_{33}) + \Omega_c\rho_{21} + \Omega_a^*\rho_{41} = 0, \tag{A1f}$$

$$\left(i\frac{\partial}{\partial t} + d_{41}\right)\rho_{41} + \Omega_a\rho_{31} - \Omega_p\rho_{43} - \mathcal{N}_\alpha \int d^3\mathbf{r}' V(\mathbf{r}' - \mathbf{r})\rho_{44,41}(\mathbf{r}', \mathbf{r}, t) = 0, \tag{A1g}$$

$$\left(i\frac{\partial}{\partial t} + d_{32}\right)\rho_{32} + \Omega_p\rho_{12} + \Omega_c(\rho_{22} - \rho_{33}) + \Omega_a^*\rho_{42} = 0, \tag{A1h}$$

$$\left(i\frac{\partial}{\partial t} + d_{42}\right)\rho_{42} + \Omega_a\rho_{32} - \Omega_c\rho_{43} - \mathcal{N}_\alpha \int d^3\mathbf{r}' V(\mathbf{r}' - \mathbf{r})\rho_{44,42}(\mathbf{r}', \mathbf{r}, t) = 0, \tag{A1i}$$

$$\left(i\frac{\partial}{\partial t} + d_{43}\right)\rho_{43} + \Omega_a(\rho_{33} - \rho_{44}) - \Omega_p^*\rho_{41} - \Omega_c^*\rho_{42} - \mathcal{N}_\alpha \int d^3\mathbf{r}' V(\mathbf{r}' - \mathbf{r})\rho_{44,43}(\mathbf{r}', \mathbf{r}, t) = 0, \tag{A1j}$$

with $d_{\alpha\beta} = \Delta_\alpha - \Delta_\beta + i\gamma_{\alpha\beta}$ and $\gamma_{\alpha\beta} = (\Gamma_\alpha + \Gamma_\beta)/2 + \gamma_{\alpha\beta}^{\mathrm{dep}}$. Here $\Gamma_\beta = \sum_{\alpha<\beta} \Gamma_{\alpha\beta}$, with $\Gamma_{\alpha\beta}$ being the spontaneous emission decay rate and $\gamma_{\alpha\beta}^{\mathrm{dep}}$ the dephasing rate from the state $|\beta\rangle$ to the state $|\alpha\rangle$. Note that, in the above equations for the one-body density matrix elements $\rho_{\alpha\beta}$, two-body density matrix elements $\rho_{\alpha\beta,\mu\nu}(\mathbf{r}', \mathbf{r}, t) \equiv \langle \hat{S}_{\alpha\beta}(\mathbf{r}', t)\hat{S}_{\mu\nu}(\mathbf{r}, t)\rangle$ are involved. Thereby, to solve Eq. (A1), one needs to solve also the equations of the two-body density matrix elements $\rho_{\rho_{\alpha\beta},\mu\nu}$, which will involve three-body density matrix elements, and so on. Equations for the two-body and three-body density matrix elements are too lengthy and thus are omitted here.

2. Derivation of the nonlinear envelope equation

We first focus on the equations of the one-body density matrix elements $\rho_{\alpha\beta}$ presented above. We employ the method of multiple scales and the approach of the beyond mean-field approximation developed in Refs. [52,54,55] to solve the MB equations (A1) and (4). To this end, we make the asymptotic expansions $\Omega_p = \sum_{j=1} \epsilon^j \Omega_p^{(j)}$ and $\rho_{\alpha\beta} = \delta_{\alpha 1}\delta_{\beta 1} + \sum_{j=1} \epsilon^j \rho_{\alpha\beta}^{(j)}$. Here ϵ is a small parameter characterizing the typical amplitude of the probe field, $\Omega_p^{(j)}$ and $\rho_{\alpha\beta}^{(j)}$ are functions of the multiple-scale variables $z_j = \epsilon^j z$ ($j = 0, 1, 2$), $t_j = \epsilon^j t$ ($j = 0, 1$), $x_1 = \epsilon x$, and $y_1 = \epsilon y$. Substituting these expansions into Eqs. (A1) and (4) and comparing powers of ϵ, we obtain a set of equations for different orders, which can be solved order by order. Note that, to derive the nonlinear envelope equation (6), the key is to get the solution of ρ_{31} up to the third-order approximation of the probe field, i.e., $\rho_{31} = \epsilon\rho_{31}^{(1)} + \epsilon^2\rho_{31}^{(2)} + \epsilon^3\rho_{31}^{(3)}$.

(i) First-order approximation. The solution of the probe field at this order has the form $\Omega_p^{(1)} = F \exp[i(Kz_0 - \omega t_0)]$, where $F = F(\mathbf{r}_1, t_1, z_2)$ [with $\mathbf{r}_1 = (x_1, y_1, z_1)$] is an envelope function undetermined yet and $K(\omega)$ is the linear dispersion relation given by formula (5). The solution of nonzero matrix elements at this order reads $\rho_{21}^{(1)} = a_{21}^{(1)}F \exp[i(Kz_0 - \omega t_0)]$, $\rho_{31}^{(1)} = a_{31}^{(1)}F \exp[i(Kz_0 - \omega t_0)]$, and $\rho_{41}^{(1)} = a_{41}^{(1)}F \exp[i(Kz_0 - \omega t_0)]$, where $a_{21}^{(1)}$, $a_{31}^{(1)}$, and $a_{41}^{(1)}$ are determined by the equation

$$\begin{pmatrix} \omega + d_{21} & \Omega_c^* & 0 \\ \Omega_c & \omega + d_{31} & \Omega_a^* \\ 0 & \Omega_a & \omega + d_{41} \end{pmatrix} \begin{pmatrix} a_{21}^{(1)} \\ a_{31}^{(1)} \\ a_{41}^{(1)} \end{pmatrix} = \begin{pmatrix} 0 \\ -1 \\ 0 \end{pmatrix}. \tag{A2}$$

Thus, we have $a_{21}^{(1)} = \Omega_c^*(\omega + d_{41})/D(\omega)$, $a_{31}^{(1)} = -(\omega + d_{21})(\omega + d_{41})/D(\omega)$, and $a_{41}^{(1)} = \Omega_a(\omega + d_{21})/D(\omega)$, where $D(\omega) = (\omega + d_{21})(\omega + d_{31})(\omega + d_{41}) - |\Omega_a|^2(\omega + d_{21}) - |\Omega_c|^2(\omega + d_{41})$.

(ii) Second-order approximation. A solvability condition at this order gives the equation

$$i\left(\frac{\partial F}{\partial z_1} + \frac{1}{V_g}\frac{\partial F}{\partial t_1}\right) = 0, \tag{A3}$$

where $V_g = (\partial K/\partial \omega)^{-1}$ is the group velocity of the probe-field envelope. The solutions of nonzero matrix elements at this order are found to be $\rho_{21}^{(2)} = a_{21}^{(2)}\partial F/\partial t_1 e^{i(Kz_0 - \omega t_0)}$, $\rho_{31}^{(2)} = a_{31}^{(2)}\partial F/\partial t_1 e^{i(Kz_0 - \omega t_0)}$, $\rho_{41}^{(2)} = a_{41}^{(2)}\partial F/\partial t_1 e^{i(Kz_0 - \omega t_0)}$, $\rho_{32}^{(2)} = \alpha_{32}^{(2)}|F|^2$, $\rho_{42}^{(2)} = a_{42}^{(2)}|F|^2$, $\rho_{43}^{(2)} = a_{43}^{(2)}|F|^2$, and

$\rho_{\alpha\alpha}^{(2)} = a_{\alpha\alpha}^{(2)}|F|^2$ ($\alpha = 1, 2, 3, 4$). Here $a_{21}^{(2)}$, $a_{31}^{(2)}$, and $a_{41}^{(2)}$ read as

$$a_{21}^{(2)} = -i\frac{(\omega+d_{31})(\omega+d_{41})-|\Omega_a|^2}{D}a_{21}^{(1)} + i\frac{(\omega+d_{41})\Omega_c^*}{D}a_{31}^{(1)} - i\frac{\Omega_c^*\Omega_a^*}{D}a_{41}^{(1)}, \tag{A4a}$$

$$a_{31}^{(2)} = i\frac{(\omega+d_{41})\Omega_c}{D}a_{21}^{(1)} - i\frac{(\omega+d_{21})(\omega+d_{41})}{D}a_{31}^{(1)} + i\frac{(\omega+d_{21})\Omega_a^*}{D}a_{41}^{(1)}, \tag{A4b}$$

$$a_{41}^{(2)} = -i\frac{\Omega_c\Omega_a}{D}a_{21}^{(1)} + i\frac{(\omega+d_{21})\Omega_a}{D}a_{31}^{(1)} - i\frac{(\omega+d_{21})(\omega+d_{31})-|\Omega_c|^2}{D}a_{41}^{(1)}, \tag{A4c}$$

and $a_{32}^{(2)}$, $a_{42}^{(2)}$, and $a_{43}^{(2)}$ satisfy the equation

$$\begin{pmatrix} d_{32} & \Omega_a^* & 0 \\ \Omega_a & d_{42} & -\Omega_c \\ 0 & -\Omega_c^* & d_{43} \end{pmatrix} \begin{pmatrix} a_{32}^{(2)} \\ a_{42}^{(2)} \\ a_{43}^{(2)} \end{pmatrix} = \begin{pmatrix} \Omega_c(a_{33}^{(2)} - a_{22}^{(2)}) - a_{12}^{(1)} \\ 0 \\ \Omega_a(a_{44}^{(2)} - a_{33}^{(2)}) + a_{41}^{(1)} \end{pmatrix}. \tag{A5}$$

Here $a_{\alpha\alpha}^{(2)}$ ($\alpha = 1, 2, 3, 4$) satisfy the equation

$$\begin{pmatrix} 0 & \Gamma_{12} & \Gamma_{13} & 0 \\ 0 & -\Gamma_{12} & \Gamma_{23} & 0 \\ 0 & 0 & -\Gamma_{13}-\Gamma_{23} & \Gamma_{34} \\ 1 & 1 & 1 & 1 \end{pmatrix} \begin{pmatrix} a_{11}^{(2)} \\ a_{22}^{(2)} \\ a_{33}^{(2)} \\ a_{44}^{(2)} \end{pmatrix} = \begin{pmatrix} 2\text{Im}(a_{31}^{(1)}) \\ 2\text{Im}(\Omega_c^* a_{32}^{(2)}) \\ 2\text{Im}(a_{31}^{(1)*} + \Omega_c a_{32}^{(2)*} + \Omega_a^* a_{43}^{(2)}) \\ 0 \end{pmatrix}. \tag{A6}$$

By solving these two equations, the explicit expressions of $a_{32}^{(2)}$, $a_{42}^{(2)}$, $a_{43}^{(2)}$, and $a_{\alpha\alpha}^{(2)}$ can be obtained.

(iii) Third-order approximation. The solution of $\rho_{\alpha 1}^{(3)}$ ($\alpha = 2, 3, 4$) can be obtained from the equation

$$\begin{pmatrix} \omega + d_{21} & \Omega_c^* & 0 \\ \Omega_c & \omega + d_{31} & \Omega_a^* \\ 0 & \Omega_a & \omega + d_{41} \end{pmatrix} \begin{pmatrix} \rho_{21}^{(3)} \\ \rho_{31}^{(3)} \\ \rho_{41}^{(3)} \end{pmatrix}$$

$$= \begin{pmatrix} a_{23}^{(2)} \\ a_{33}^{(2)} - a_{11}^{(2)} \\ a_{43}^{(2)} \end{pmatrix} |F|^2 F e^{i(Kz_0 - \omega t_0)} + \begin{pmatrix} 0 \\ 0 \\ \mathcal{N}_a \int \mathbf{r}_1' V(\mathbf{r}_1' - \mathbf{r}_1)\rho_{44,41}^{(3)}(t_0, z_0, \mathbf{r}_1', \mathbf{r}_1, t_1, z_2) \end{pmatrix}. \tag{A7}$$

Notice that to obtain the solutions of $\rho_{31}^{(3)}$, equations for some two-body density matrix elements $\rho_{\alpha\beta,\mu\nu}$ must be solved. These two-body density matrix elements are nonzero starting at the second order, so they can be assumed to have the form $\rho_{\alpha\beta,\mu\nu} = \epsilon^2\rho_{\alpha\beta,\mu\nu}^{(2)} + \epsilon^3\rho_{\alpha\beta,\mu\nu}^{(3)} + \cdots$. The second-order solution has the form $\rho_{\alpha 1,\beta 1}^{(2)} = a_{\alpha 1,\beta 1}^{(2)}|\Omega_p|^2$ ($\alpha, \beta = 2, 3, 4$), where $a_{\alpha 1,\beta 1}^{(2)}$ satisfy the following equations:

$$\begin{pmatrix} \omega + d_{21} & 0 & 0 & \Omega_c^* & 0 & 0 \\ 0 & \omega + d_{31} & 0 & \Omega_c & 0 & \Omega_a^* \\ 0 & 0 & \omega + d_{41} - V/2 & 0 & 0 & \Omega_a \\ \Omega_c & \Omega_c^* & 0 & 2\omega + d_{21} + d_{31} & \Omega_a^* & 0 \\ 0 & 0 & 0 & \Omega_a & 2\omega + d_{21} + d_{41} & \Omega_c^* \\ 0 & \Omega_a & \Omega_a^* & 0 & \Omega_c & 2\omega + d_{31} + d_{41} \end{pmatrix} \begin{pmatrix} a_{21,21}^{(2)} \\ a_{31,31}^{(2)} \\ a_{41,41}^{(2)} \\ a_{21,31}^{(2)} \\ a_{21,41}^{(2)} \\ a_{31,41}^{(2)} \end{pmatrix} = -\begin{pmatrix} 0 \\ a_{31}^{(1)} \\ 0 \\ a_{21}^{(1)} \\ 0 \\ a_{41}^{(1)} \end{pmatrix}. \tag{A8}$$

With these results, the third-order equations of the two-body density matrix elements (which are too lengthy and thus are not written explicitly down here) can be solved, which have the solution of the form $\rho_{\alpha\beta,\mu\nu}^{(3)} = a_{\alpha\beta,\mu\nu}^{(3)}|\Omega_p(\mathbf{r}', t)|^2\Omega_p(\mathbf{r}, t)$, where $a_{\alpha\beta,\mu\nu}^{(3)}$ are functions of $\mathbf{r}' - \mathbf{r}$ and ω. The solution of $\rho_{44,41}^{(3)}$ can be written as $\rho_{44,41}^{(3)}(\mathbf{r}_1', \mathbf{r}_1, t_0, t_1) = a_{44,41}^{(3)}|F(\mathbf{r}_1', t_1)|^2 F(\mathbf{r}_1, t_1)e^{i(Kz_0 - \omega t_0)}$, with

$$a_{44,41}^{(3)} = \frac{A_0 + A_1 V(\mathbf{r}' - \mathbf{r}) + A_2 V(\mathbf{r}' - \mathbf{r})^2 + A_3 V(\mathbf{r}' - \mathbf{r})^3}{B_0 + B_1 V(\mathbf{r}' - \mathbf{r}) + B_2 V(\mathbf{r}' - \mathbf{r})^2 + B_3 V(\mathbf{r}' - \mathbf{r})^3 + B_4 V(\mathbf{r}' - \mathbf{r})^4}. \tag{A9}$$

Here A_n and B_n ($n = 0, 1, 2, 3, 4$) are complex constants depending on the spontaneous emission decay rate $\Gamma_{\alpha\beta}$, the dephasing rate $\gamma_{\alpha\beta}^{\text{dep}}$, the detuning Δ_α, and the half Rabi frequencies Ω_a and Ω_c; their explicit expressions are too lengthy and thus are omitted here.

With the expression of $a_{44,41}^{(3)}$ at hand, we can acquire the solution of $\rho_{31}^{(3)}$ up to the third-order approximation through solving Eq. (A7). Then, from the solutions of $\rho_{31}^{(1)}$, $\rho_{31}^{(2)}$, and $\rho_{31}^{(3)}$ given above and by a solvability condition, we obtain the nonlinear equation for the envelope function F:

$$i\frac{\partial F}{\partial z_2} = -\frac{1}{2k_p}\left(\frac{\partial^2 F}{\partial x_1^2} + \frac{\partial^2 F}{\partial y_1^2}\right) + \frac{K_2}{2}\frac{\partial^2 F}{\partial t_1^2} + \int d^3\mathbf{r}_1' H(\mathbf{r}_1' - \mathbf{r}_1)|F(\mathbf{r}_1', z_2, t_1)|^2 F(\mathbf{r}_1, z_2, t_1), \tag{A10}$$

where $H(\mathbf{r}_1' - \mathbf{r}_1) = \kappa_{13}\mathcal{N}_a d_{21}\Omega_a^* a_{44,41}^{(3)}(\mathbf{r}_1' - \mathbf{r}_1, \omega)/D(\omega)$ is the nonlocal nonlinear response function contributed by the Rydberg-Rydberg interaction. Last, combining Eqs. (A3) and (A10), we obtain Eq. (6) in the main text.

[1] J. Lu and J. F. Greenleaf, Nondiffracting X waves-exact solutions to free-space scalar wave equation and their finite aperture realizations, IEEE Trans. Ultrason. Ferroelectron. Freq. Control **39**, 19 (1992).

[2] J. Lu and J. F. Greenleaf, Experimental verification of non-diffracting X waves, IEEE Trans. Ultrason. Ferroelectron. Freq. Control **39**, 441 (1992).

[3] A. C. Newell and J. V. Moloney, *Nonlinear Optics* (Addison-Wesley, Redwood City, 1992).

[4] Y. S. Kivshar and G. P. Agrawal, *Optical Solitons: From Fibers to Photonic Crystals* (Academic, San Diego, 2003).

[5] B. A. Malomed, D. Mihalache, F. Wise, and L. Torner, Spatiotemporal optical solitons, J. Opt. B: Quantum Semiclassical Opt. **7**, R53 (2005).

[6] H. E. Hernández-Figueroa, M. Zamboni-Rached, and E. Recami, *Localized Waves* (Wiley, Hoboken, NJ, 2008).

[7] M. Kolesik, E. M. Wright, and J. V. Moloney, Dynamic Nonlinear X Waves for Femtosecond Pulse Propagation in Water, Phys. Rev. Lett. **92**, 253901 (2004).

[8] A. Porras, A. Dubietis, E. Kučinskas, F. Bragheri, V. Degiorgio, A. Couairon, D. Faccio, and P. Di Trapani, From X- to O-shaped spatiotemporal spectra of light filaments in water, Opt. Lett. **30**, 3398 (2005).

[9] C. Conti, S. Trillo, G. Valiulis, A. Piskarskas, O. Jedrkiewicz, J. Trull, and P. Di Trapani, Nonlinear Electromagnetic X Waves, Phys. Rev. Lett. **90**, 170406 (2003).

[10] C. Conti, Generation and nonlinear dynamics of X waves of the Schrödinger equation, Phys. Rev. E **70**, 046613 (2004).

[11] P. Di Trapani, G. Valiulis, A. Piskarskas, O. Jedrkiewicz, J. Trull, C. Conti, and S. Trillo, Spontaneously Generated X-Shaped Light Bullets, Phys. Rev. Lett. **91**, 093904 (2003).

[12] D. N. Christodoulides, N. K. Efremidis, P. Di Trapani, and B. A. Malomed, Bessel X waves in two- and three-dimensional bidispersive optical systems, Opt. Lett. **29**, 1446 (2004).

[13] P. V. Larsen, M. P. Sørensen, O. Bang, W. Z. Królikowski, and S. Trillo, Nonlocal description of X waves in quadratic nonlinear materials, Phys. Rev. E **73**, 036614 (2006).

[14] H. Xu and H. Zeng, Elliptic X-shaped light bullets, Opt. Lett. **32**, 820 (2007).

[15] H. Xu and H. Zeng, Spontaneously generated walking X-shaped light bullets, Opt. Lett. **32**, 1944 (2007).

[16] M. A. Porras and A. Parola, Breakup of self-guided light beams into X wave trains, Opt. Lett. **33**, 2656 (2008).

[17] W. Lei, J. Wu, H. Cai, and H. Zeng, Nonlinear X-shaped waves by second-harmonic generation with collimated femtosecond pulses, Opt. Lett. **34**, 166 (2009).

[18] G. Valiulis, V. Jukna, O. Jedrkiewicz, M. Clerici, E. Rubino, and P. Di Trapani, Propagation dynamics and X-pulse formation in phase-mismatched second-harmonic generation, Phys. Rev. A **83**, 043834 (2011).

[19] F. Baronio, S. Chen, M. Onorato, S. Trillo, S. Wabnitz, and Y. Kodama, Spatiotemporal optical dark X solitary waves, Opt. Lett. **41**, 5571 (2016).

[20] S. Longhi and D. Janner, X-shaped waves in photonic crystals, Phys. Rev. B **70**, 235123 (2004).

[21] Y. Lahini, E. Frumker, Y. Silberberg, S. Droulias, K. Hizanidis, R. Morandotti, and D. N. Christodoulides, Discrete X-Wave Formation in Nonlinear Waveguide Arrays, Phys. Rev. Lett. **98**, 023901 (2007).

[22] P. G. Kevrekidis, J. Gagnon, D. J. Frantzeskakis, and B. A. Malomed, X, Y, and Z waves: Extended structures in nonlinear lattices, Phys. Rev. E **75**, 016607 (2007).

[23] M. Heinrich, A. Szameit, F. Dreisow, R. Keil, S. Minardi, T. Pertsch, S. Nolte, and A. Tünnermann, Observation of Three-Dimensional Discrete-Continuous X Waves in Photonic Lattices, Phys. Rev. Lett. **103**, 113903 (2009).

[24] N. K. Efremidis, N. S. Nye, and D. N. Christodoulides, Exact bidirectional X-wave solutions in fiber Bragg gratings, Phys. Rev. A **96**, 043820 (2017).

[25] K. B. Chung, Propagation of Bessel-X pulses in a hybrid photonic crystal, J. Mod. Opt. **65**, 1033 (2018).

[26] W. Kan, B. Liang, X. Zhu, J. Tu, X. Zou, and J. Cheng, Non-propagating X-shaped acoustic waves in sonic crystals without defects, Appl. Phys. Lett. **97**, 223504 (2010).

[27] C. Conti and S. Trillo, Nonspreading Wave Packets in Three Dimensions Formed by an Ultracold Bose Gas in an Optical Lattice, Phys. Rev. Lett. **92**, 120404 (2004).

[28] D. Colas, F. P. Laussy, and M. J. Davis, Formation of nonlinear X-waves in condensed matter systems, Phys. Rev. B **99**, 214301 (2019).

[29] E. S. Sedov, I. V. Iorsh, S. M. Arakelian, A. P. Alodjants, and A. Kavokin, Hyperbolic Metamaterials with Bragg Polaritons, Phys. Rev. Lett. **114**, 237402 (2015).

[30] O. Voronych, A. Buraczewski, M. Matuszewski, and M. Stobińska, Exciton-polariton localized wave packets in a microcavity, Phys. Rev. B **93**, 245310 (2016).

[31] A. Gianfrate, L. Dominici, O. Voronych, M. Matuszewski, M. Stobińska, D. Ballarini, M. D. Giorgi, G. Gigli, and D. Sanvitto, Superluminal X-waves in a polariton quantum fluid, Light: Sci. Appl. **7**, 17119 (2018).

[32] J. Lu and S. He, Optical X wave communications, Opt. Commun. **161**, 187 (1999).

[33] M. Ornigotti, C. Conti, and A. Szameit, Effect of Orbital Angular Momentum on Nondiffracting Ultrashort Optical Pulses, Phys. Rev. Lett. **115**, 100401 (2015).

[34] T. F. Gallagher, *Rydberg Atoms* (Cambridge University, Cambridge, England, 2008).

[35] M. Saffman, T. G. Walker, and K. Mølmer, Quantum information with Rydberg atoms, Rev. Mod. Phys. **82**, 2313 (2010).

[36] J. D. Pritchard, K. J. Weatherill, and C. S. Adams, Nonlinear optics using cold Rydberg atoms, Annu. Rev. Cold At. Mol. **1**, 301 (2013).

[37] O. Firstenberg, C. S. Adams, and S. Hofferberth, Nonlinear quantum optics mediated by Rydberg interactions, J. Phys. B: At., Mol. Opt. Phys. **49**, 152003 (2016).

[38] C. Murray and T. Pohl, Quantum and nonlinear optics in strongly interacting atomic ensembles, in *Advances in Atomic, Molecular, and Optical Physics* (Academic, New York, 2016), Vol. 65, Chap. 7, pp. 321–372.

[39] M. Fleischhauer, A. Imamoglu, and J. P. Marangos, Electromagnetically induced transparency: Optics in coherent media, Rev. Mod. Phys. **77**, 633 (2005).

[40] W. Krolikowski, O. Bang, and J. Wyller, Modulational instability in nonlocal nonlinear Kerr media, Phys. Rev. E **64**, 016612 (2001).

[41] J. Wyller, W. Krolikowski, O. Bang, and J. J. Rasmussen, Generic features of modulational instability in nonlocal Kerr media, Phys. Rev. E **66**, 066615 (2002).

[42] W. Królikowski, O. Bang, N. I. Nikolov, D. Neshev, J. Wyller, J. J. Rasmussen, and D. Edmundson, Modulational instability, solitons and beam propagation in spatially nonlocal nonlinear media, J. Opt. B. **6**, S288 (2004).

[43] E. V. Doktorov and M. A. Molchan, Modulational instability in nonlocal Kerr-type media with random parameters, Phys. Rev. A **75**, 053819 (2007).

[44] N. Henkel, R. Nath, and T. Pohl, Three-Dimensional Roton Excitations and Supersolid Formation in Rydberg-Excited Bose-Einstein Condensates, Phys. Rev. Lett. **104**, 195302 (2010).

[45] F. Maucher, N. Henkel, M. Saffman, W. Królikowski, S. Skupin, and T. Pohl, Rydberg-Induced Solitons: Three-Dimensional Self-Trapping of Matter Waves, Phys. Rev. Lett. **106**, 170401 (2011).

[46] S. Sevincli, N. Henkel, C. Ates, and T. Pohl, Nonlocal Nonlinear Optics in Cold Rydberg Gases, Phys. Rev. Lett. **107**, 153001 (2011).

[47] B. K. Esbensen, A. Wlotzka, M. Bache, O. Bang, and W. Krolikowski, Modulational instability and solitons in nonlocal media with competing nonlinearities, Phys. Rev. A **84**, 053854 (2011).

[48] F. Maucher, S. Skupin, and W. Krolikowski, Collapse in the nonlocal nonlinear Schrödinger equation, Nonlinearity **24**, 1987 (2011).

[49] L. Tiofack, H. Tagwo, O. Dafounansou, A. Mohamadou, and T. C. Kofane, Modulational instability in nonlocal media with competing non-Kerr nonlinearities, Opt. Commun. **357**, 7 (2015).

[50] F. Maucher, T. Pohl, S. Skupin, and W. Krolikowski, Self-Organization of Light in Optical Media with Competing Nonlinearities, Phys. Rev. Lett. **116**, 163902 (2016).

[51] F. Maucher, T. Pohl, W. Krolikowski, and S. Skupin, Pattern formation in the nonlinear Schrödinger equation with competing nonlocal nonlinearities, Opt. Data Process. Storage **3**, 13 (2017).

[52] Z. Bai, W. Li, and G. Huang, Stable single light bullets and vortices and their active control in cold Rydberg gases, Optica **6**, 309 (2019).

[53] We assume that all the atoms are initially populated in the ground state $|1\rangle$, and hence the average of the operator $\hat{O}$ means $\langle\hat{O}\rangle = \langle G|\hat{O}|G\rangle$, with $|G\rangle = |1, 1, 1, \ldots, 1\rangle$.

[54] Z. Bai and G. Huang, Enhanced third-order and fifth-order Kerr nonlinearities in a cold atomic system via atom-atom interaction, Opt. Express **24**, 4442 (2016).

[55] C. Hang, W. Li, and G. Huang, Nonlinear light diffraction by electromagnetically induced gratings with $\mathcal{PT}$ symmetry in a Rydberg atomic gas, Phys. Rev. A **100**, 043807 (2019).

[56] S. Mauger, J. Millen, and M. P. A. Jones, Spectroscopy of strontium Rydberg states using electromagnetically induced transparency, J. Phys. B **40**, F319 (2007).

[57] K. G. Makris, Z. H. Musslimani, D. N. Christodoulides, and S. Rotter, Constant-intensity waves and their modulation instability in non-Hermitian potentials, Nat. Commun. **6**, 7257 (2015).

[58] For deriving the external potential (17), we have assumed that the gradient of the magnetic field is of ϵ^3 order, i.e., $(B_1, B_2) = \epsilon^3(B_1^{(3)}, B_2^{(3)})$, and hence the gradient magnetic field $B(x, y) = \epsilon^3(B_1^{(3)}x + B_2^{(3)}y) = \epsilon^2(B_1^{(3)}x_1 + B_2^{(3)}y_1)$.

[59] L. Karpa and M. Weitz, A Stern-Gerlach experiment for slow light, Nat. Phys. **2**, 332 (2006).

[60] Y. Guo, L. Zhou, L.-M. Kuang, and C. P. Sun, Magneto-optical Stern-Gerlach effect in an atomic ensemble, Phys. Rev. A **78**, 013833 (2008).

[61] C. Hang and G. Huang, Stern-Gerlach effect of weak-light ultraslow vector solitons, Phys. Rev. A **86**, 043809 (2012).